



Contents lists available at ScienceDirect

Biosensors and Bioelectronics

journal homepage: www.elsevier.com/locate/bios

Wireless portable bioelectronic nose device for multiplex monitoring toward food freshness/spoilage

Kyung Ho Kim^{a,1}, Dongseok Moon^{b,1}, Jai Eun An^{a,c,1}, Seon Joo Park^a, Sung Eun Seo^a, Siyoung Ha^a, Jinyeong Kim^a, Kayoung Kim^d, Sooyeol Phyo^{e,f}, Jiwon Lee^{e,g}, Hye-Yeon Kim^{h,i}, Moonil Kim^j, Tai Hyun Park^{b,c,**}, Hyun Seok Song^{d,***}, Oh Seok Kwon^{a,k,*}

^a Infectious Disease Research Center, Korea Research Institute of Bioscience and Biotechnology (KRIBB), Daejeon, 34141, Republic of Korea

^b School of Chemical and Biological Engineering, Institute of Chemical Processes, Seoul National University, Seoul, 08826, Republic of Korea

^c Interdisciplinary Program in Bioengineering, Seoul National University, Seoul, 08826, Republic of Korea

^d Sensor System Research Center, Korea Institute of Science and Technology, Seoul, 02792, Republic of Korea

^e Center for Sustainable Environment Research, Korea Institute of Science and Technology (KIST), Seoul, 02792, Republic of Korea

^f Department of Materials Science and Engineering, Korea University, Seoul, 02841, Republic of Korea

^g Division of Energy & Environment Technology, Korea University of Science and Technology (UST), 217 Gajeong-ro, Yuseong-gu, Daejeon, 34113, Republic of Korea

^h Research Center for Bioconvergence Analysis, Korea Basic Science Institute, Cheongju, Chungbuk, 28119, Republic of Korea

ⁱ Center for Convergent Research of Emerging Virus Infection (CEVI), Korea Research Institute of Chemical Technology, Daejeon, 34114, Republic of Korea

^j Bionanotechnology Research Center, Korea Research Institute of Bioscience and Biotechnology (KRIBB), 125 Gwahang-ro, Yuseong-gu, Daejeon, 34141, South Korea

^k Nanobiotechnology and Bioinformatics (Major), University of Science & Technology (UST), 125 Gwahak-ro, Yuseong-gu, Daejeon, 34141, South Korea

ARTICLE INFO

Keywords:

Electronic nose
Olfactory receptor
Biogenic amines
Gas sensor
Gas monitoring
Portable device

ABSTRACT

Monitoring food freshness/spoilage is important to ensure food quality and safety. Current methods of food quality monitoring are mostly time-consuming and labor intensive processes that require massive analytical equipment. In this study, we developed a portable bioelectronic nose (BE-nose) integrated with trace amine-associated receptor (TAAR) nanodiscs (NDs), allowing food quality monitoring via the detection of food spoilage indicators, including the biogenic amines cadaverine (CV) and putrescine (PT). The olfactory receptors TAAR13c and TAAR13d, which have specific affinities for CV and PT, were produced and successfully reconstituted in ND structures. TAAR13 NDs BE-nose-based side-gated field-effect transistor (SG-FET) system was constructed by utilizing a graphene micropattern (GM) into which two types of olfactory NDs (TAAR13c ND and TAAR13d ND) were introduced, and this system showed ultrahigh sensitivity for a limit of detection (LOD) of 1 fM for CV and PT. Moreover, the binding affinities between the TAAR13 NDs and the indicators were confirmed by a tryptophan fluorescence quenching assay and biosimulations, in which the specific binding site was confirmed. Gas-phase indicators were detected by the TAAR13 NDs BE-nose platform, and the LODs for CV and PT were confirmed to be 26.48 and 7.29 ppb, respectively. In addition, TAAR13 NDs BE-nose was fabricated with commercial gas sensors as a portable platform for the measurement of NH₃ and H₂S, multiplexed monitoring was achieved with similar performance, and the change ratio of the indicators was observed in a real sample. The integration of commercial gas sensors on a BE-nose enhanced the accuracy and reliability for the quality monitoring of real food samples. These results indicate that the portable TAAR13 NDs BE-nose can be used to monitor CV and PT over a wide range of concentrations, therefore, the electronic nose platform can be utilized for monitoring the freshness/spoilage step in various foods.

* Corresponding author. Infectious Disease Research Center, Korea Research Institute of Bioscience and Biotechnology (KRIBB), Daejeon, 34141, Republic of Korea.

** Corresponding author. School of Chemical and Biological Engineering, Institute of Chemical Processes, Seoul National University, Seoul, 08826, Republic of Korea.

*** Corresponding author. Sensor System Research Center, Korea Institute of Science and Technology, Seoul, 02792, Republic of Korea.

E-mail addresses: thpark@snu.ac.kr (T.H. Park), hssong@kist.re.kr (H.S. Song), oskwon79@kribb.re.kr, oskwon7799@gmail.com (O.S. Kwon).

¹ These authors contributed equally to this work.

<https://doi.org/10.1016/j.bios.2022.114551>

Received 10 April 2022; Received in revised form 22 June 2022; Accepted 5 July 2022

Available online 8 July 2022

0956-5663/© 2022 Elsevier B.V. All rights reserved.

1. Introduction

Food safety is a major concern in the worldwide, in both the food industry and the healthcare system (Ruiz-Capillas and Herrero, 2019). In particular, among numerous information of the food products in both consumer and modern society, food spoilage is the main issue because of the critical negative effect on humans of food containing unsafe microorganisms (Xu et al., 2017). For example, meat is a perishable food that usually deteriorates rapidly, within a few days (Kaale et al., 2011). Meat spoilage progresses in time via biochemical and physicochemical transformations (Rukchon et al., 2014). In the biochemical spoilage process of meat, decarboxylation of amino acids by bacteria generates biogenic amines (Dave and Ghaly, 2011; Halász et al., 1994). In addition, the amino acids in meat can be degraded into simple compounds such as NH_3 and H_2S by hydrolysis (Rukchon et al., 2014). These biogenic amines and small chemical compounds produced by the deterioration of meat can be used as spoilage indicators. Targets indicating the freshness of food are normally complex mixtures; therefore, the development of monitoring tools offering multiplexed platforms for the detection of these spoilage indicators with high selectivity is required.

Trace amine-associated receptors (TAARs) are G protein-coupled receptors (GPCRs) that recognize biogenic amines (Liberles, 2009). TAARs have been reported to function as vertebrate olfactory receptors. The kinds of TAARs vary between species, with 6 in humans (hTAARs), 15 in mice (mTAARs), 6 in macaques (macTAARs) and 112 in zebrafish (zTAARs) (Liberles, 2015). In particular, the TAAR13c and TAAR13d in zebrafish (*Danio rerio*) have been reported to selectively bind to death-associated odorants such as cadaverine (CV) and putrescine (PT) (Hussain et al., 2013; Li et al., 2015; Xu and Li, 2020). CV and PT are biogenic amines that are produced by the microbial decarboxylation of amino acids (Xu and Li, 2020). CV and PT are formed by the decarboxylation of lysine and ornithine, respectively (Dave and Ghaly, 2011; Halász et al., 1994). There have been reports that the mass of CV and PT increases with the incubation time of fresh meat, such as pork, beef, sausage, anchovy and tuna (Bover-Cid et al., 2001; Draisci et al., 1998; Halász et al., 1994; Shalaby, 1996). For this reason, CV and PT have been suggested as chemical indicators of meat spoilage, and monitoring the concentrations of the generated biogenic amines is important for determining food freshness and spoilage (Triki et al., 2018).

To date, various methods for CV and PT detection have been developed, such as cyclic voltammetry, resistance, colorimetry, polymerase chain reaction (PCR), fluorescence, gas chromatography–mass spectrometry (GC–MS), liquid chromatography–mass spectrometry (LC–MS), surface-enhanced Raman spectroscopy (SERS), chemiluminescence, and field-effect transistors (FETs) (De Las Rivas et al., 2006; H. Kim et al., 2021; Ma et al., 2018; Morsy et al., 2016; Schaude et al., 2017; Semeano et al., 2018; Siripongpreda et al., 2020; Valdez et al., 2019). However, these techniques have limitations such as high cost, time-consuming, large instruments, low sensitivity, and low selectivity. Although in our previous report, CV and PT were detected using SERS with-Au functionalized metal-organic frameworks (MOFs), which showed high performance, this technique still suffered from low repeatability, low reproducibility and nonspecificity toward other biogenic amines because its mechanism is based on absorption (H. Kim et al., 2021). In addition, although the various electronic noses (E-noses) have been developed for the detection or analysis of various gases in the various food samples, E-nose is absent for detection or real-time monitoring toward CV and PT (Castrica et al., 2019; Leopold et al., 2016; Nimsuk, 2019; Ying et al., 2017; Zheng et al., 2016). Therefore, the development of a sensor platform for high-sensitivity and high-selectivity detection of CV and PT still remains challenging.

The production of transmembrane proteins, such as GPCRs, in *Escherichia coli* (*E. coli*) systems has been widely used because it is effective for mass production and is cost-effective. However, reconstitution of the structure of GPCRs is challenging because almost all GPCRs produced in *E. coli* system are expressed as inclusion bodies (Heim et al.,

2021; Serebryany et al., 2012; Yang et al., 2015). For this reason, reconstitution techniques have been developed to recover the functionality of GPCRs, such as the use of detergent micelles, liposomes, bicelles and nanodiscs (NDs) (Goddard et al., 2015; Kiefer et al., 1996; Wang and Tonggu, 2015). Among these materials, NDs have been considered the most effective reconstitution material because of their stability in various environments and their functional lifetimes (Denisov and Sligar, 2016, 2017). For these reasons, NDs have been applied in many functional and structural studies (Rouck et al., 2017). NDs are composed of three components: receptors to detect target molecules, lipid bilayers to form native lipid membrane environments and membrane scaffold proteins (MSPs) to tightly wrap the edge of the lipid bilayer. In previous studies, the TAAR13c ND-based BE-nose offered selective and sensitive detection of CV with high stability in aqueous and gaseous phases (Oh et al., 2019a; Yang et al., 2017). However, not only CV but also other components such as PT, NH_3 , and H_2S are major indicators for monitoring food spoilage.

In this study, we first developed a device for on-site and in-situ utilization based on a wireless portable TAAR13 NDs BE-nose integrated with commercial gas sensors for multiplexed monitoring of CV, PT, NH_3 , and H_2S . In particular, TAAR13c and TAAR13d, as olfactory receptors were utilized for specific recognition of the biogenic amines and were reconstituted with NDs to improve their functionality. In addition, the interfacial chemical bis(2-aminoethylene)perylene-3,4,9,10-tetracarboxyldiimide (PDA) was introduced to decrease steric hindrance and improve of the immobilization efficiency of TAAR13 NDs (Kim et al., 2020b). The binding energies between TAAR13 NDs and the indicators were determined to be -0.14171 eV and -0.14588 eV for the interactions between TAAR13c and CV and between TAAR13d and PT, respectively, using biosimulations. The real-time responses of side-gated field-effect transistors (SG-FETs) toward various indicators showed high sensitivity and selectivity, and the limit of detection (LOD) was 1 fM for CV and PT. In the gas sensor system, the LODs were 26.48 ppb for CV and 7.29 ppb for PT, indicating high performance. In addition, for the first time, a wireless portable TAAR13 NDs BE-nose integrated with commercial gas sensors allowed multiple monitoring of spoilage indicators from real food samples and showed high-performance and sensitivity. Our sensor system opens up the possibility of a portable TAAR13 NDs BE-nose system for on-site and in-situ freshness/spoilage monitoring.

2. Materials and methods

2.1. Cloning of TAAR13c and TAAR13d genes into expression vectors

TAAR13c gene was obtained from zebrafish (*Danio rerio*) cDNA by PCR with primers (5' ATG AAT TCA TGG ATT TAT CAT CAC AAG AAT 3' and 5' ATC TCG AGT CAA ACC GTA AAT AAA TTG ATA 3') for mammalian expression and (5' CAC CAG GAG ATA TAC ATA TGA TGC CCT TTT GCC ACA AT 3' and 5' TGA ACT CAA TTC CAA AAA TAA TTT ACA C 3') for bacterial expression. The TAAR13c gene was cloned into mammalian expression vector pcDNA3 and the bacterial expression vector pET-DEST42 (Invitrogen). The TAAR13d gene was synthesized for codon optimization in a bacterial expression system (Bionics). Additionally, the TAAR13d gene was cloned into the mammalian expression vector pcDNA3 and the bacterial expression vector pET-DEST42 (Invitrogen).

2.2. Nano-glo dual luciferase reporter assay

Nano-glo dual luciferase reporter assay (Promega) was applied for characterization of TAAR13c and TAAR13d receptors. We used *firefly* luciferase as a reporter to measure the response of olfactory receptors and NanoLuc® luciferase for constitutively expressed control reporter. A total of 1.5×10^4 HEK293T cells were transferred into 96-well plates and cultured in Dulbecco's modified Eagle's medium (DMEM) (HyClon)

containing 1% penicillin, 1% streptomycin (Gibco), and 10% fetal bovine serum (FBS) (Gibco) at 37°C under 5% CO₂. After 24 h, olfactory receptors and other accessory proteins were transfected at a fixed ratio (pCRE-luc:pNL:M3R:RTP1S:Ric8b: *G_{αolf}*:OR) = 2:1:2:2:1:1:10) with Lipofectamine 3000 (Invitrogen). After transfection, the medium was replaced with 50 μL CD293 with 1X GlutaMAX™ (Gibco) and the plates were incubated for 30 min at 37°C. The plates were incubated for 4 h at 37°C after odorant stimulation. The luminescence was measured by Spark™ 10 M multimode microplate reader (TECAN). The normalized luciferase activity was calculated with the formula $[\text{CRE/NL(N)} - \text{CRE/NL(0)}]/[\text{CRE/NL(FSK)} - \text{CRE/NL(0)}]$. Forskolin (FSK)-treated cells (10 μM) were used as a positive control and odorant-untreated cells (0) were used as a negative control.

2.3. Purification of olfactory receptors

The Rosetta™ 2 (DE3) *E. coli* strain (Merck) was used for production of all proteins. SuptoxD and SuptoxR which coexpress DjIA and RraA, respectively, were used to overexpress olfactory receptors. The olfactory receptor gene was transformed into *E. coli* and incubated in 100 μg/mL ampicillin and 40 μg/mL chloramphenicol agar plates for 16 h at 37°C. A single colony was inoculated into 5 mL LB medium containing antibiotics (100 μg/mL ampicillin and 40 μg/mL chloramphenicol) and incubated for 16 h at 37°C. The bacterial cells were inoculated into 1 L fresh LB medium and incubated until the OD₆₀₀ value reached 0.3–0.5 at 30°C after 0.2% arabinose induction. The temperature was decreased to 25°C, and 0.1 mM IPTG was added to the medium to induce the expression of olfactory receptors. After incubating the medium for 16 h at 25°C, the cells were harvested by centrifugation (4°C, 7000 g, 15 min) and resuspended in PBS buffer containing 2 mM EDTA (pH 7.4). The insoluble fraction of cell lysates was obtained by sonication (5 s on/off, 38% amplitude, 5 min) and centrifugation (4°C, 12000 g, 30 min). The insoluble fraction was solubilized with solubilization buffer (0.1 M Tris-HCl, 20 mM SDS, 1 mM EDTA, 0.1 M DTT, pH 8.0) and incubated at 30°C overnight. The solubilized proteins were obtained by centrifugation (20°C, 12 000 g, 30 min) and dialyzed by dialysis membrane tubing (MEMBRA-CEL®, 14 kDa cutoff) with binding buffer (0.1 M sodium phosphate, 10 mM SDS, pH 8.0). The olfactory receptor was purified by HisTrap™ HP column (GE Healthcare) using washing buffer (0.1 M sodium phosphate, 10 mM SDS, pH 7.0) and elution buffer (0.1 M sodium phosphate, 10 mM SDS, pH 6.0). We exchanged the buffer of the purified olfactory receptor with HEPES buffer I (20 mM HEPES, 100 mM NaCl, 25 mM cholate, pH 8.0) by HiTrap™ Desalting column (GE Healthcare) for assembly of NDs.

2.4. Purification of a membrane scaffold protein (MSP1E3D1)

The membrane scaffold protein gene (pMSP1E3D1 (Addgene)) was transformed into *E. coli* and incubated in 50 μg/mL kanamycin agar plates for 16 h at 37°C. A single colony was inoculated into 5 mL LB medium containing antibiotics (50 μg/mL kanamycin) and incubated for 16 h at 37°C. The bacterial cells were inoculated into 1 L fresh LB medium and incubated until the OD₆₀₀ value reached 0.5 at 37°C. Expression of MSP1E3D1 was induced by 1 mM IPTG and the cells were incubated for 4 h at 37°C. The cells were harvested by centrifugation (4°C, 7000 g, 15 min) and resuspended in binding buffer (20 mM Tris-HCl, 0.5 M NaCl, 20 mM imidazole pH 8.0). The supernatant of cell lysates was obtained by sonication (5 s on/off, 38% amplitude, 5 min) and centrifugation (4°C, 12000 g, 30 min). The supernatant was applied to a HisTrap™ HP column (GE Healthcare) and purified by using washing buffer (20 mM Tris-HCl, 0.5 M NaCl, 50 mM imidazole pH 8.0) and elution buffer (20 mM Tris-HCl, 0.5 M NaCl, 350 mM imidazole pH 8.0). The buffer of purified MSP1E3D1 was exchanged with HEPES buffer II (20 mM HEPES, 100 mM NaCl, pH 8.0) by a HiTrap™ Desalting column (GE Healthcare) for assembly of nanodiscs. To cleave off the

histidine tag of MSP1E3D1, purified MSP1E3D1 was incubated with TEV protease at a molar ratio of 1:100 for 16 h at 4°C. Truncated MSP1E3D1 was obtained from the flow-through of a HisTrap™ HP column.

2.5. Assembly and purification of olfactory receptor-embedded NDs

DMPC (20 mM) in HEPES buffer (20 mM HEPES, 100 mM NaCl, 50 mM cholate, pH 8.0) was used for assembly of olfactory receptor-embedded NDs. MSP1E3D1 was added to the DMPC solution at a 1:150 M ratio, and the mixture was incubated for 10 min at 24°C. The olfactory receptor in HEPES buffer I was added to the mixture, and the mixture was incubated for 2 h at 24°C. The final molar ratio of olfactory receptor, MSP1E3D1 and DMPC was 1:5:750. To remove cholate, 0.5 g Bio-Beads (Bio-Rad)/mL of mixture assembly was added to the mixture, and the mixture was incubated for 16 h at 24°C. To remove empty NDs, the mixture was applied to a HisTrap™ HP column and purified by HEPES elution buffer (20 mM HEPES, 100 mM NaCl, 350 mM imidazole pH 8.0). Size exclusion chromatography (Superdex 200 Increase 10/300 GL, GE Healthcare) was used to purify olfactory receptor-embedded NDs with optimal size.

2.6. SDS-PAGE analysis

An acrylamide gel loaded with purified protein or ND samples was incubated with Coomassie Blue staining solution (Coomassie Blue 0.5 g/L, acetic acid 7% (v/v), methanol 40% (v/v)) for 1 h at room temperature. The gel was destained by destaining solution I (acetic acid 7% (v/v), methanol 40% (v/v)) for 1 h at room temperature and destaining solution II (acetic acid 7% (v/v), methanol 5% (v/v)) overnight at room temperature. Anti-V5 epitope tag mouse antibody (Santa Cruz Biotechnology) was used as a primary antibody for detecting olfactory receptors and HRP-conjugated anti-mouse antibody (Merck) was used as a secondary antibody in Western blot analysis.

2.7. Tryptophan fluorescence quenching assay

The functionality of olfactory receptor-embedded NDs was analyzed by means of a tryptophan fluorescence quenching assay using a luminescence spectrometer (LS 55 Luminescence Spectrometer, PerkinElmer). We excited the NDs at 290 nm and detected the emission at 350 nm. The normalized fluorescence intensity was calculated with the formula $(\Delta F/F_0) (\%) = [(F_0 - F)/F_0] \times 100 (\%)$. F_0 is fluorescence intensity of odorant-untreated NDs and F is fluorescence intensity of odorant-treated NDs.

2.8. Size analysis of olfactory receptor-embedded ND

The size of the NDs was analyzed by a DLS spectrophotometer (DLS-7000). The measurement conditions for DLS were as follows; temperature (25°C), refractive index (1.3315), and viscosity (0.891). Field-emission scanning electronic microscopy (AURIGA, Carl Zeiss) was used to analyze the size analysis of olfactory-receptor-embedded NDs and their shape.

2.9. Fabrication of the TAAR13 NDs BE-nose

Larger-scale (7 × 7 cm) graphene was fabricated by chemical vapor deposition (CVD), and the fabricated graphene on copper foil was transferred onto a silicon dioxide (SiO₂) wafer using a wet-transfer process. The electrodes were fabricated by a microelectromechanical system (MEMS), such as spin coating of a photoresist (GXR-601, AZ electronic materials and DNR L300-40, Dongjin Semichemichem Co., Ltd.), reactive-ion etching (etcher, RIE 80 plus, Oxford instrument) for graphene micropatterning, photolithography (MA-6, Karl-Suss Microtec) for electrode patterning, deposition (ZZS550-2/D, Maestech) for electrode formation and dicing (DAD 3350, Disco), and passivation of

the electrodes as SiO₂ layers using a sputtering system (KVS-5000, KVT Co., Ltd) to prevent nonspecific binding. For immobilization of the TAAR13 NDs, 10 µL 20 µM PDA was dropped on the graphene micro-pattern (GM) and reacted for 1 h at RT (K. H. Kim et al., 2021). The PDA-immobilized GM was treated with 10 µL 2% glutaraldehyde (GA) over 4 h at 4°C and washed using PBS solution and DW. Finally, 10 µL 1 µM TAAR13 NDs was treated on GA/PDA-immobilized GM over 12 h at 4°C and then cleaned using PBS solution and DW.

2.10. Electrical measurements of the TAAR13 NDs BE-nose

All electrical measurements were carried out by a Keithley 2612 A source meter, the current and resistance were normalized by equations (1) and (3), respectively.

$$\Delta R/R_0 = (R-R_0)/R_0 \quad (3)$$

where R_0 is the initial resistance and R is the instantaneously measured resistance in real-time.

2.11. Performance of biosimulations

Ligand binding sites were docked using Autodock 4.0, and the resulting morphology was analyzed along with basic parameters. PyMOL was used to visualize and graphically represent ligand binding results in various ways.

2.12. Preparation of gaseous samples

The standard CV and PT gases were collected using a gas generation system that consisted of a pressure regulator, bubbler chamber, mass flow controller (MFC), and gas chamber⁵¹. Each 2.24 M CV and PT solution was diluted by the serial dilution method, and the solution was loaded into a bubbler chamber. The vaporized gases were generated from a standard solution using the flow into the 100 sccm N₂, and then the vaporized gases were pushed to the gas chamber using 500 sccm N₂, and the final gases were collected in a 1 L Tedlar bag. A 50 g real sample was loaded in a 2 L chamber, and the gases were collected in a 1 L Tedlar bag through the connecting tube using a vacuum pump every day.

2.13. GC-FID analysis of CV and PT

The solid-phase microextraction (SPME) fiber holder and assembly of 100 µm PMDS were purchased from Supelco Inc. (Bellefonte, PA). The SPME fibers were conditioned for 30 min at 250°C in the GC injector. The fibers were injected and transferred into the Tedlar bag in 5 min for sampling CV and PT, respectively. The fibers were then removed and inserted into the injector of a 7820 A gas chromatograph (Agilent Technologies) equipped with FID. A total of 10 m of Rtx-5MS column (0.25 mm, thickness 0.10 µm) was used with the following temperature program: for PT and CV, the oven temperature was 70°C and then increased at 15°C/min to 100°C, where it was held 1 min. The calibration procedure was performed as follows: a 1 L Tedlar bag was thoroughly cleaned by flushing the nitrogen gas. The calibration samples were prepared by transferring an aliquot of PT and CV liquid into a Tedlar bag, diluting with nitrogen gas sequentially, and then analyzing by the same procedure for the sample from the bubbler instrument. The software used for data recording and analysis was Agilent OpenLAB CDS ChemStation Edition Rev. C.01.08.

2.14. FT-IR spectroscopy for NH₃ measurement

FT-IR gas experiments for NH₃ were performed with a MATRIX-MG5 (Bruker, Germany) instrument. The gas samples collected from the Tedlar bag were directly transferred into the inlet of the FT-IR spectrophotometer using a vacuum pump at a flow rate of 100 sccm. FT-IR

spectra were recorded in the range of 4000–400 cm⁻¹, and then the range of 950–1000 cm⁻¹ was selected for calculation of the NH₃ concentration. The software used for data recording and analysis was OPUS GA v5.2.10.26.

2.15. PTR-ToF-MS for H₂S measurement

The concentration of H₂S was measured with PTR-ToF-MS (VOCUS 2 R, Aerodyne Research Inc., United States). All samples were directly transferred for 5 min into the inlet of the PTR-ToF-MS instrument through perfluoroalkoxy alkane (PFA) tubing at a flow rate of 100 sccm. Mass spectra were recorded for mass-to-charge (m/z) ratios of 1–500 m/z at a rate of 1 Hz, using H₃O⁺ as the primary reagent ion and an electric field to number density ratio (E/N) of 100×10^{-17} V cm². The large segmented quadrupole (BSQ) voltage of PTR-ToF-MS was adjusted to 150 V due to the low detection limit of H₂S. The peak at 34.995 m/z (H₂SH⁺) was used for the quantification of H₂S, and the reference gases were generated in the laboratory for the calibration curve. The recorded ToF data were analyzed using the Tofware software package (Aerodyne Research Inc., United States).

3. Results

Fig. 1 presents an illustration of the overall freshness/spoilage monitoring system based on the TAAR13 NDs and commercial gas sensor integrated with a portable device. The olfactory receptor NDs, as specific bioprobes toward freshness/spoilage, were introduced onto the surface of a graphene channel via the interfacial chemical PDA. Commercial gas sensors were utilized to determine the degree of spoilage by monitoring NH₃ and H₂S. In addition, the NDs in the TAAR 13 NDs BE-nose exhibited high affinity for CV and PT, with high sensitivity and selectivity. The BE-nose was integrated with a disposable sim chip, which was inserted into a portable device containing commercial gas sensors of the multiplex monitoring for spoilage indicators, CV, PT, NH₃, and H₂S.

3.1. Characterization of TAAR13c and TAAR13d

It was reported that TAAR13c and TAAR13d, originating from zebrafish, interact specifically with CV and PT (Hussain et al., 2013; Li et al., 2015; Xu and Li, 2020). We confirmed their properties including their affinity and selectivity to CV and PT using luciferase reporter assay that has been widely applied for studying the function of GPCRs (Li and Matsunami, 2011; Saito et al., 2009; Zhuang and Matsunami, 2007, 2008). In this assay, HEK293T cells expressing TAAR13c and TAAR13d responded to the death-associated odorants, CV and PT, respectively, in a dose-dependent manner (Fig. 2a and b). Additionally, we performed a selectivity test to confirm that olfactory receptors specifically bind to the death-associated odorants. We chose different biogenic amines or amino acids containing monoamines or diamines (Fig. 2c). HEK293T cells expressing TAAR13c responded to CV, and cells expressing TAAR13d responded to both CV and PT (Fig. 2d). A similar result in terms of the selectivity of TAAR13c and TAAR13d to these biogenic amines has been shown in a previous study (Li et al., 2015).

3.2. Production of TAAR13c and TAAR13d-embedded NDs

We used the *E. coli* strains coexpressing either DjlA, a the membrane-bound DnaK cochaperone, or RraA, an inhibitor of the mRNA-degrading activity of *E. coli* RNase E, to suppress protein-induced toxicity and overexpress the olfactory receptors in a bacterial system (Gialama et al., 2017a, 2017b; Michou et al., 2019). The *E. coli* strain coexpressing DjlA was termed SuptoxD and the *E. coli* strain coexpressing RraA was termed SuptoxR. We collected samples during the purification of TAAR13c expressed in wild-type cells. Sodium dodecyl sulfate-polyacrylamide gel electrophoresis (SDS-PAGE) analysis of the samples showed the high

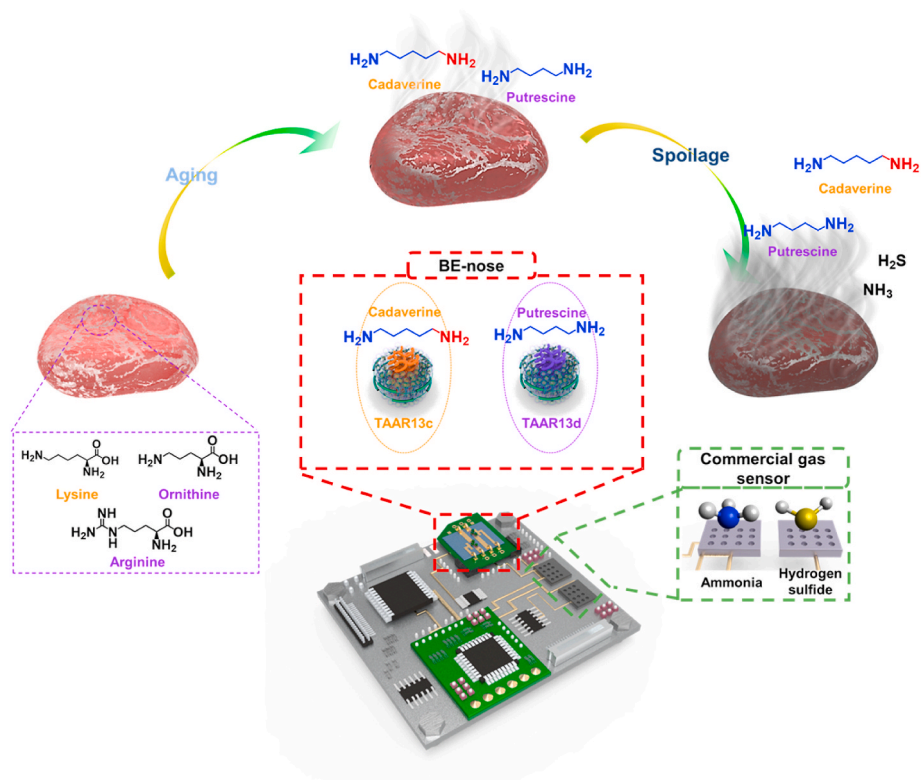


Fig. 1. Overall concept of a portable BE-nose. Schematic illustration of spoilage indicator detection from meat using wireless portable BE-nose.

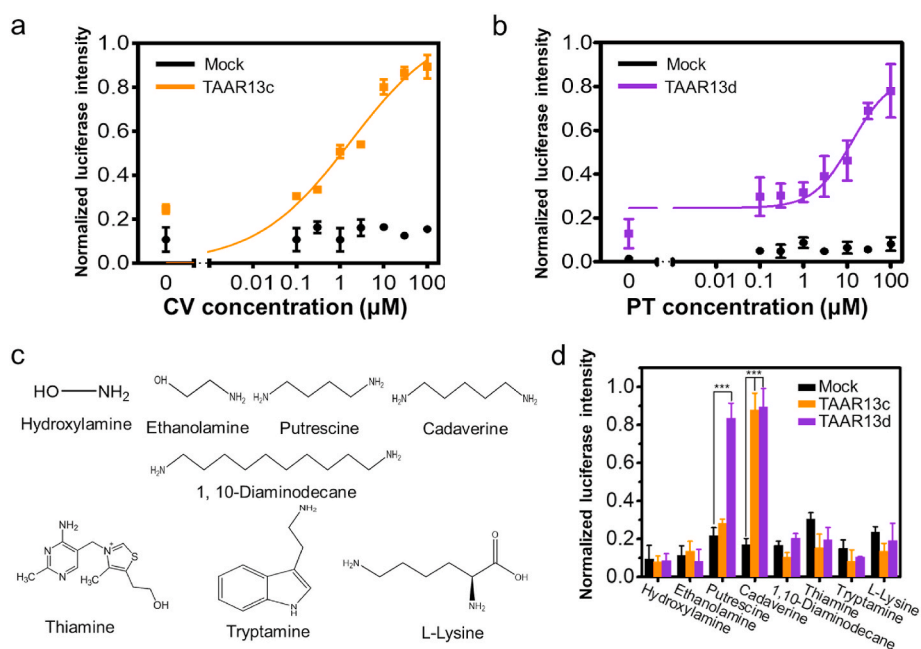


Fig. 2. Characterization of TAAR13c and TAAR13d expressed in HEK293T cells. Dose-dependent responses of a TAAR13c to CV and b TAAR13d to PT. c Chemical structures of various biogenic amines for the selectivity test. d Selectivity test of TAAR13c and TAAR13d to various biogenic amines. The error bars represent the standard error of the mean ($n = 3$, $***P < 0.001$).

purity but low content of TAAR13c in the eluent lane (E) (Fig. S1a). The contents of TAAR13c and TAAR13d were increased in both SuptoxD and SuptoxR cells (Fig. S1b). SuptoxR cells expressing TAAR13c after 0.1 mM IPTG induction and SuptoxR cells expressing TAAR13d after 0.5 mM IPTG induction showed the highest productivity in the experimental group (Fig. S1c). The purified TAAR13c and TAAR13d overexpressed in

SuptoxR were confirmed by SDS-PAGE analysis (Fig. 3a) and Western blot analysis (Figs. S2a and S2b). In the SuptoxR cells, the production of the olfactory receptors caused lower protein-induced toxicity to the host cell than that in SuptoxD cells.

TAAR13 NDs were prepared using purified olfactory receptors, lipid bilayers, and membrane scaffold proteins (MSPs) via a facile self-

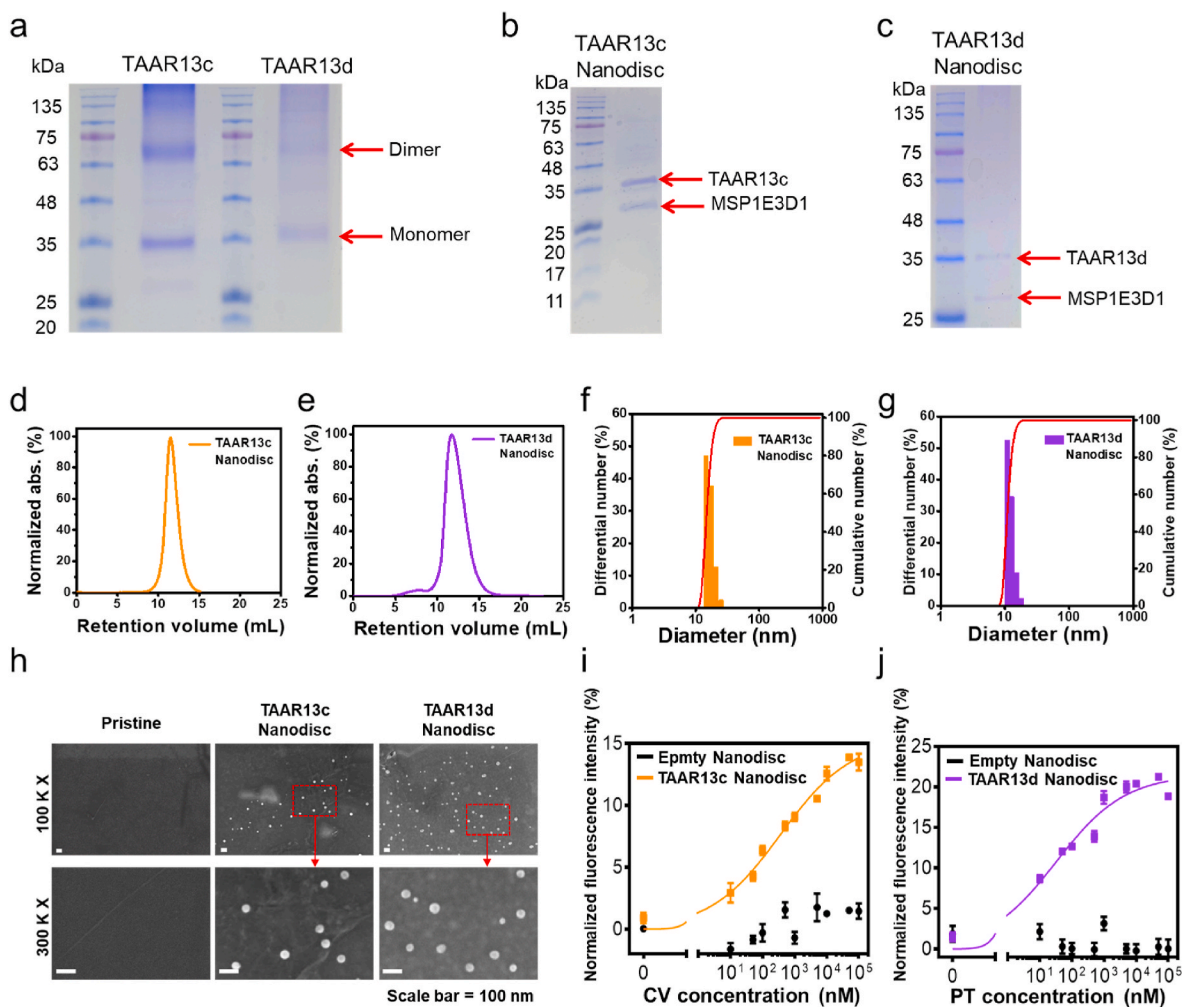


Fig. 3. Purification of olfactory receptors produced in *E. coli* and characterization of olfactory receptor-embedded NDs. **a** Coomassie blue staining analysis of purified TAAR13c and TAAR13d from *E. coli*. Coomassie blue staining analysis of purified **b** TAAR13c ND and **c** TAAR13d ND. Size-exclusion chromatography profiles of **d** TAAR13c ND and **e** TAAR13d ND. Dynamic light scattering profiles of **f** TAAR13c ND and **g** TAAR13d ND. **h** FE-SEM images of pristine graphene (left), TAAR13c ND (middle) and TAAR13d ND (right). Tryptophan fluorescence quenching assay for dose-dependent responses of **i** TAAR13c ND to CV and **j** TAAR13d ND to PT. The error bars represent the standard error of the mean ($n = 3$).

assembly process described in our previous studies (Oh et al., 2019a; Yang et al., 2017). We optimized the size of the olfactory receptor-embedded NDs in terms of the molar ratios of the ND components (Hagn et al., 2018). The optimal ratio of the olfactory receptor, MSP1E3D1 and DMPC was 1:5:750. The absorbance peak of the olfactory receptor-embedded NDs was observed at a retention volume of approximately 12 mL (Fig. 3d and e) (Ma et al., 2017). The size distribution and homogeneity of the olfactory receptor-embedded NDs were analyzed by dynamic light scattering (DLS). The average diameters of TAAR13c NDs (Fig. 3f) and TAAR13d NDs (Fig. 3g) were 16.7 nm and 12.2 nm, respectively. The field-emission scanning electron microscopy (FE-SEM) images clearly demonstrated that the shape of the olfactory receptor-embedded NDs was a discoidal disc (Fig. 3h). These results clearly demonstrate that the NDs were successfully self-assembled in homogeneous discoidal shapes with proper size.

The composition of the olfactory receptors and MSP1E3D1 in the NDs was confirmed by SDS-PAGE analysis (Fig. 3b and c). The TAAR13c and TAAR13d bands were observed at approximately 38 kDa, and the MSP1E3D1 band was observed at approximately 30 kDa. The olfactory receptors within the TAAR13c and TAAR13d NDs were confirmed by Western blot analysis using an anti-V5 tag antibody (Figs. S2c and S2d).

To analyze the functionality and affinity of TAAR13 NDs for biogenic amines, a tryptophan fluorescence assay was carried out. It is known

that the binding of functional receptors to selective ligands quenches the intrinsic fluorescence of the receptors (Kim et al., 2019; Son et al., 2017; Yang et al., 2015). The TAAR13c NDs and TAAR13d NDs exhibited dose-dependent responses to CV and PT, respectively, while the empty NDs did not bind to these death-associated odorants (Fig. 3i and j). TAAR13c NDs could detect CV with an EC_{50} of 370 nM and TAAR13d NDs could detect PT with an EC_{50} of 33 nM. The EC_{50} of these death-associated-odorants to the respective NDs indicated that the binding affinity of TAAR13d NDs to PT was approximately 10 times stronger than that of TAAR13c NDs to CV. These results are consistent with previous studies (Li et al., 2015; Xu and Li, 2020) and demonstrated that the TAAR13 NDs were prepared successfully and can be utilized as recognition elements in BE-noses for the efficient detection of biogenic amines.

3.3. Characterization of the TAAR13 NDs BE-nose

To investigate the TAAR13c ND- and TAAR13d ND-conjugated onto graphene, Fourier transform infrared (FT-IR) spectroscopy was performed for analysis of the amide bond between the amine group of PDA and the carboxylic acid group of the TAAR13 NDs (Kim et al., 2020b). The absorption spectra showed an amide I band at approximately 1530 cm^{-1} and an amide II band at approximately 1760 cm^{-1} , and broad

bands corresponding to $-OH$ and $-NH$ groups were confirmed between 3600 cm^{-1} to 3100 cm^{-1} . The vibrations of the amine, alkyl and carbonyl groups corresponded to the absorption peaks in the range from 1700 cm^{-1} to 1200 cm^{-1} , and the sharp and strong $C-N$ and $C-O$ bands were observed in the 1400 cm^{-1} to 1200 cm^{-1} and 1700 cm^{-1} to 1480 cm^{-1} regions, respectively (Fig. 4a).

The electrodes of the 4-inch wafer scale were fabricated by a microelectromechanical system (MEMS) for the TAAR13 NDs BE-nose (Fig. 4b). The electrode consisted of a graphene-based dual-channel including a source/drain, a side gate for the field-effect, and the immobilized TAAR13 NDs. The graphene surface was modified for bioreceptor immobilization as previously described, and the bioreceptors were immobilized onto interfacial chemical linker-treated graphene via the formation of amide bonds (Fig. 4b insert).

The electrical properties of the TAAR13 NDs BE-nose were first evaluated by plotting current-voltage (I - V) curves in the range from -2.5 V to 2.5 V (scan rate = 0.1 Vms^{-1}) for the graphene-immobilized TAAR13 NDs. Although the I - V curves exhibited a decreased slope (pristine graphene of 0.71 to 0.488 in TAAR13c ND and 0.365 in TAAR13d ND) caused by immobilization on the modified surface, the I - V curves obviously showed a stable ohmic contact (Fig. 4c) (Park et al., 2020).

The illustration in Fig. 4d indicates a dual-channel SG-FET, which is composed of a 3-ternary system of a side gate, a source, and drain electrodes to measure the electrical transport in real-time. In addition, the chamber was filled with a phosphate-buffered saline (PBS, pH 7.4) solution as a dielectric material, which generated a field-effect by

supplying voltage via the side-gate electrode.

The TAAR13-conjugated BE-nose was excellently operated as an FET channel and was shown to be a transducer for signal amplification, as demonstrated by the transfer curves (I_{ds} - V_g) (Kwon et al., 2015; Park et al., 2020). In addition, the graphene field-effect transistors exhibited ambipolar conductance, in the p-type region, the sensor platform was stably operated and had enhanced sensing performance according to previous studies (Fig. 4e) (Fujimoto and Awaga, 2013; Kwon et al., 2013).

3.4. Real-time monitoring of TAAR13 NDs SG-FET

To confirm the spoilage indicator detection performance of TAAR13 NDs-conjugated SG-FET platforms, dual GM channels were conjugated with TAAR13c ND and TAAR13d ND for CV and PT detection, respectively. The real-time responses were in terms of the concentrations of CV and PT, and the current change was normalized by the equation

$$\Delta I / I_0 = (I - I_0) / I_0 \quad (1)$$

where I and I_0 represent the instantaneous current changes after exposure to the target indicators and the initial current, respectively (Fig. 4f and g). Control experiments were carried out with empty NDs without receptors, such as TAAR13c or TAAR13d, to confirm the interaction between the receptors and the target indicators, which obviously showed no electrical signal (black line). Fig. 4f displays the real-time response of TAAR13c ND SG-FETs toward various concentrations of

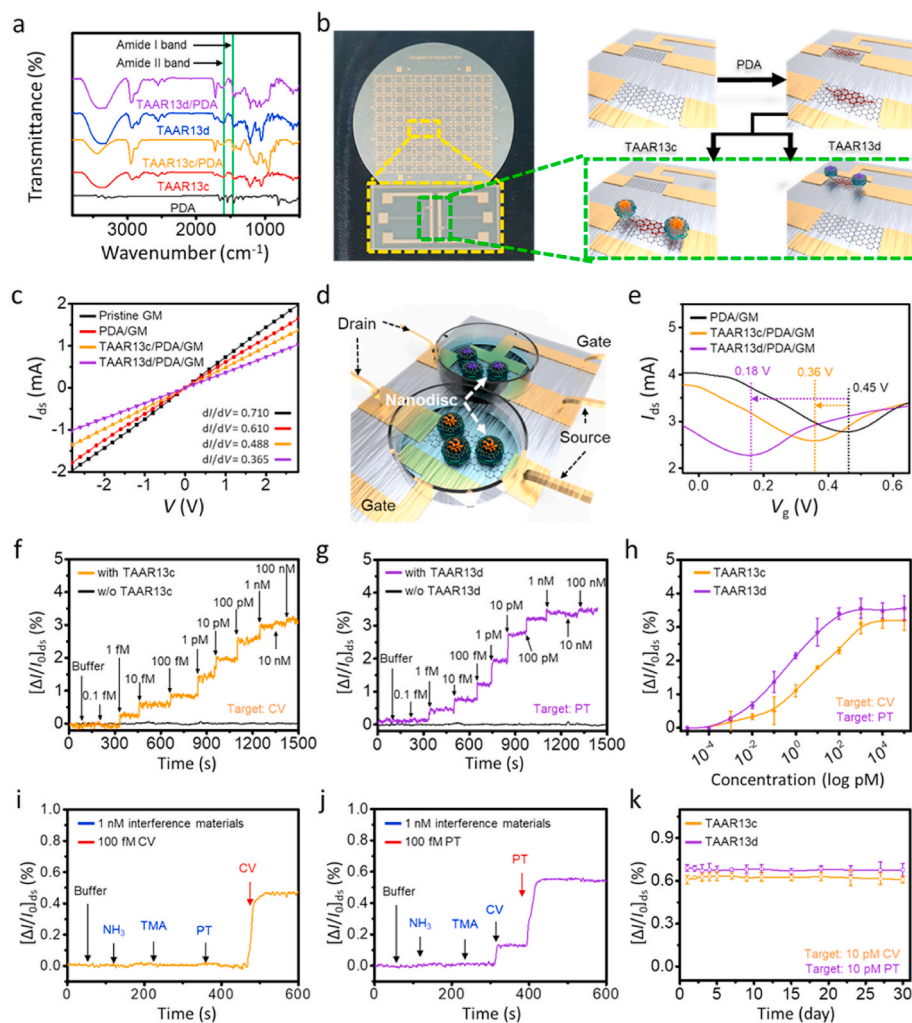


Fig. 4. Characterization and electrical measurements of TAAR13 NDs SG-FETs in the liquid phase. a FT-IR spectrum of each TAAR13 NDs immobilization step with the linker and TAAR13 NDs on the graphene surface. b Photographs of TAAR13 NDs SG-FET electrodes on the wafer scale and a piece (yellow dot square). Schematic diagram of the surface modification step. c I - V curves for the surface modification. d Schematic illustrations of the dual-channel liquid-ion-gated FET system for multidetection. e Transfer curves of TAAR13 NDs SG-FETs (TAAR13c ND; orange, TAAR13d ND; violet). Real-time responses of TAAR13 NDs SG-FETs to various concentrations of f CV and g PT. h Calibration curves of the TAAR13 NDs SG-FET of CV (orange) and PT (violet). Specific test of TAAR13 NDs SG-FET toward i CV and j TAAR13d ND SG-FET for PT. k Long-term stability of each TAAR13 NDs SG-FET towards target indicators at 4°C .

CV ranging from 0.1 fM to 100 nM. Before monitoring the electrical signal toward CV, only buffer was injected to confirm the signal, and there was no current change. On the other hand, current changes were instantly observed upon CV injection, and the TAAR13c ND SG-FETs showed a linear range of 1 fM to 1 nM and excellent performance, with an LOD of 1 fM (Kim et al., 2020a; Oh et al., 2019a). The TAAR13d ND SG-FET was monitored for detection toward various concentrations of PT in the range from 0.1 fM to 100 nM. Although buffer was injected to confirm the signal change, there was no current change. The TAAR13d ND SG-FETs exhibited a linear range from 1 fM to 100 pM and an LOD of 1 fM (Fig. 4g). The normalized sensitivities were determined by the current change level, and the concentration curves were obtained by normalizing the sensitivities depending on the concentration. The K constants were calculated by curve fitting based on Langmuir's adsorption isotherm equation (Fig. 4h)

$$N = C / (1 / K + C) \quad (2)$$

where N is the normalized sensitivity and C is the concentration of indicators (Kim et al., 2020a; Lee et al., 2011, 2020; Park et al., 2021). The K values calculated based on the concentration curves were $2.616 \times 10^{12} \text{ M}^{-1}$ for the TAAR13c ND SG-FETs and $1.748 \times 10^{13} \text{ M}^{-1}$ for the TAAR13d ND SG-FETs. The TAAR13 NDs SG-FET system could detect CV and PT at various concentrations. To confirm the specific detection of the TAAR13 NDs, first, the TAAR13 ND SG-FETs were exposed to spoilage molecules such as (NH_3 , H_2S , and PT or CV (Fig. 4i and j). The TAAR13c ND SG-FETs clearly responded to CV at a concentration of 100 fM. However, no significant responses were observed toward NH_3 , H_2S , or PT. The TAAR13c ND SG-FETs exhibited excellent sensitivity toward CV and showed no response for coexisting nontargets at concentrations 10^4 times higher than the CV concentrations (Fig. 4i). The TAAR13d ND SG-FETs showed a clear response toward 100 fM PT, as well as toward other death-associated odorants, such as trimethylamine (TMA) and NH_3 . Although CV interacted with TAAR13d ND, the TAAR13d ND were 10^4 times more sensitivity PT than to CV (with a response at 1 nM). The interactions between TAAR13d ND and CV/PT are shown in Fig. 2d (Fig. 4j).

The storage stability of the TAAR13 NDs SG-FETs was evaluated for 30 days at 4°C with 10 pM aliquots of each target, and their current changes showed excellent environmental stability, which was maintained at over 95% as shown in Fig. 4k. Functionality of TAAR13 NDs could be maintained, because the immobilization of NDs on the graphene prevented aggregation of NDs by electrostatic interactions between lipids and receptor or membrane scaffold proteins (Johansen et al., 2019; Oh et al., 2019b; Wadsäter et al., 2013). Additionally, the electrical stability test of TAAR13 NDs was performed to observe the current variant depending on the electrical affect (Fig. S3). The stable current showed in nA current range, and the unstable response exhibited μA current range owing to the occurred heat by contact resistance, which means that the high voltage and current can be affected for operating of biomolecules.

3.5. Calculation of the binding affinity between the indicators and TAAR13 NDs

To confirm the interaction between TAAR13 bioreceptors and spoilage indicators, a simulation was conducted by Autodock. Previous studies confirmed that TAAR13c is a highly sensitive and specific receptor for CV, with TAAR13d exhibiting the highest affinity for PT (Li et al., 2015). The classical amine binding motif of the amine receptor consists of Asp 112 and Asp 202 (Sharma et al., 2016), and GPCRs are known to interact with ligands through this specific moiety to form salt bridges, van der Waals interactions, and hydrogen bonds (Sharma et al., 2018). We hypothesized that these residues of TAAR13c and TAAR13d might be involved in binding to CV and PT and investigated the binding affinities between receptors and ligands by simulation. TAAR13c (3pds)

and TAAR13d (2rh1) structural models were generated using SWISS-MODEL (Biasini et al., 2014). The docking results confirmed the association of Asp 112 and Asp 202 with the ligand and TAAR binding. The amino group of CV formed a salt bridge with Asp 112 and Asp 202 in TAAR13c at distances of 2.7 Å and 3.2 Å, respectively, with a binding energy of -3.4 kcal/mol. Additionally, it formed a salt bridge in TAAR13d with a distance of 3.0 Å and a binding energy of -3.5 kcal/mol. The amino group of PT formed a salt bridge with Asp 112 in TAAR13d at a distance of 2.9 Å with a binding energy of -3.6 kcal/mol (Fig. 5a and b). The selectivity TAAR13c and TAAR13d for CV and PT indicates that distinct olfactory receptors sense different diamines.

3.6. GC analysis of spoilage gases

To monitor freshness, standard indicator gases were measured at various concentrations. CV and PT gases were formed from a gas generator and collected in a Tedlar bag to quantify their concentrations. Gas chromatography (GC) analysis was conducted using a gas chromatography-flame ionization detector (GC-FID) to analyze the generated standard CV and PT gases. Fig. 5c shows the calibration curves from the GC chromatograms, which present the liquid-phase concentration (C_L) versus the gas-phase concentration (C_G) (Fig. S4).

3.7. Electrical measurements of spoilage gases using TAAR13 NDs BE-nose

Real-time measurements were performed with the TAAR13 NDs BE-nose exposed periodically to CV gas (Fig. 5d). An abrupt resistance change was observed upon exposure to CV gas, which was proportional to the concentration, and the LOD was approximately 26.48 ppb. The NDs structure was exposed to environmental conditions for activation of the receptor in the dry state (Oh et al., 2019a). In addition, the CV gas from the NDs was detached by injection with N_2 gas thus, the resistance showed an instant change. Therefore, the TAAR13c ND BE-nose showed reversible properties, such as recovery of the resistance ratio, and reusability of the CV gas. The calibration curve was generated from the normalized sensitivity from cyclic exposure to concentrations of CV gas (Fig. 5e and S5a). Fig. 5f shows the cross-reactivity of the TAAR13c ND BE-nose toward spoilage gases such as NH_3 , H_2S and PT. No significant responses to similar concentrations of these other gases were observed. On the other hand, an obvious response to CV was observed. To confirm the performance of the TAAR13d ND BE-nose, the resistance change was measured after exposure to various concentrations of gases (Fig. 5g). When exposed to PT, the TAAR13d ND BE-nose showed an immediate response, and the sensitivity was observed to be proportional to the concentration in the range from 7.29 to 30.12 ppb. In addition, the TAAR13d ND BE-nose had a LOD of 7.29 ppb. The concentration curve ranging from 7.29 to 30.12 ppb was obtained from the real-time response of the TAAR13d ND BE-nose exposed to various concentrations of PT (Fig. 5h and S5b). The change ratio of resistance was calculated by normalization based on the resistance in Fig. 5e, and the reusability was confirmed by the results obtained upon displacing of PT by N_2 purging. Finally, the selectivity of the TAAR13d ND BE-nose was determined by exposure to diverse spoilage gases, such as NH_3 , H_2S and CV. However, the BE-nose was shown to respond specifically to the biogenic amines, CV and PT (Fig. 5i). Moreover, the selective performance of each BE-nose was carried out by exposing the various gases such as volatile organic compounds (VOCs) (Shao et al., 2018) and volatile basic nitrogen (VBN), and these results showed the excellent detection performance toward CV or PT of BE-nose (Fig. S6). Based on the results, the repeatability and reproducibility were performed using the various gases, and BE-nose showed a clear detection performance (Fig. S7).

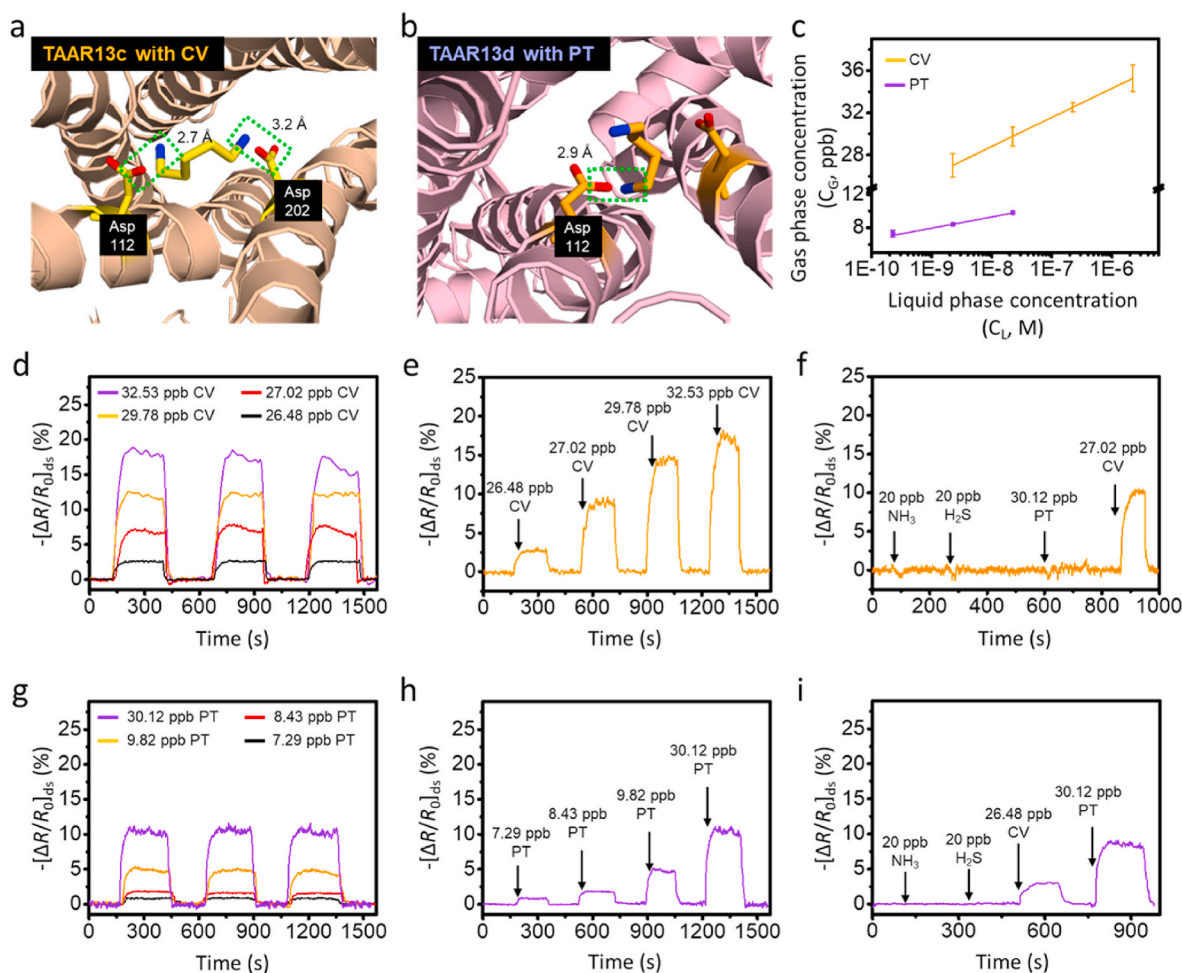


Fig. 5. Gas sensing performance of the TAAR13 NDs BE-nose. **a, b** The 3D structures obtained through simulation of the binding site marked between TAAR13 NDs and CV/PT. **c** Correlation curves between liquid phase concentration and gas phase concentration. **d** Real-time responses of TAAR13c ND BE-nose upon cyclical exposure to CV concentrations of 26.48–32.527 ppb. **e** Concentration curve depending on various CV concentrations. **f** Specificity of the TAAR13c ND BE-nose. **g** Real-time responses of the TAAR13d ND BE-nose upon cyclical exposure to PT concentrations of 7.29–30.12 ppb. **h** Concentration curve depending on various PT concentrations. **i** Specificity of the TAAR13d ND BE-nose.

3.8. Spoilage gas measurements in real samples using a portable TAAR13 NDs BE-nose

The photograph in Fig. 6a shows the covered portable TAAR13 NDs BE-nose platform for protection from various gases. The TAAR13 NDs BE-nose platform used for insertion into the portable device was composed of a TAAR13 NDs BE-nose connected to the sim chip via wire bonding, and this device was simply designed for easy replacement (Fig. 6b and S8). The scheme of TAAR13 NDs conjugation on the dual channel is presented in Fig. 6b. The print circuit board (PCB) was assembled in two layers; the sensors, such as the sim socket and the commercial gas sensors, were located on the top layer for simple replacement as other parts at the corrosion of sensors, and the rechargeable battery was located on the backside of the bottom layer (Fig. S9). A portable device was received through the various modules by signal converting such as analog-to-digital (ADC) module, digital-to-analog (DAC) module, data acquisition (DAQ) module and the signal processing module (Li et al., 2020; Wang et al., 2021; Xu et al., 2022). Real-time responses were obtained with 27.02 ppb CV and 8.43 ppb PT using a portable TAAR13 NDs BE-nose, and the results showed resistance changes similar to those observed via Keithley measurements (Fig. 6c). Therefore, the portable TAAR13 NDs BE-nose platform was considered suitable for on-site utilization by minimization of the device. To investigate the gases generated in situ (CV, PT, NH₃, and H₂S) from a

real sample, the gases were collected using a Tedlar bag and vacuum pump, and then the Tedlar bag was connected to the chamber containing the portable TAAR13 NDs BE-nose and the gases were injected into in chamber (Fig. 6d). The gas measurement was monitored via a Bluetooth connection with a tablet PC, and the user interface simply consists of 1) CV and PT monitors, 2) commercial gas sensor monitors, and 3) real-time data. Moreover, the portable TAAR13 NDs BE-nose was placed with a real sample in the chamber, and the real-time responses toward CV and PT were monitored for 1 day (Fig. 6e). The change ratio of PT in the real sample was found to be greater than that of CV, consistent with the generation pathway of biogenic amines (Fig. S10) (Halász et al., 1994; Jairath et al., 2015). For long-term monitoring of the generation ratio of indicators in a real sample, the gases were collected for 6 days, and the portable TAAR13 NDs BE-nose was exposed to the collected gases. The resistance changes toward the indicators gradually increased with time; interestingly, CV and PT showed instantly increasing signals from 3 days. However, CV and PT showed no considerable signal changes after 4 days and 5 days, respectively (Fig. 6f). Furthermore, the resistance changes of other spoilage indicators, NH₃ and H₂S, showed a gradually increasing trend with rapid increases between 4 days and 5 days (Fig. 6g). The portable TAAR13 NDs BE-nose detected spoilage indicators earlier than the commercial NH₃ and H₂S sensors and was indicated that the freshness of the real sample dramatically decayed after 3 days. The concentrations of CV and PT were analyzed by GC-FID

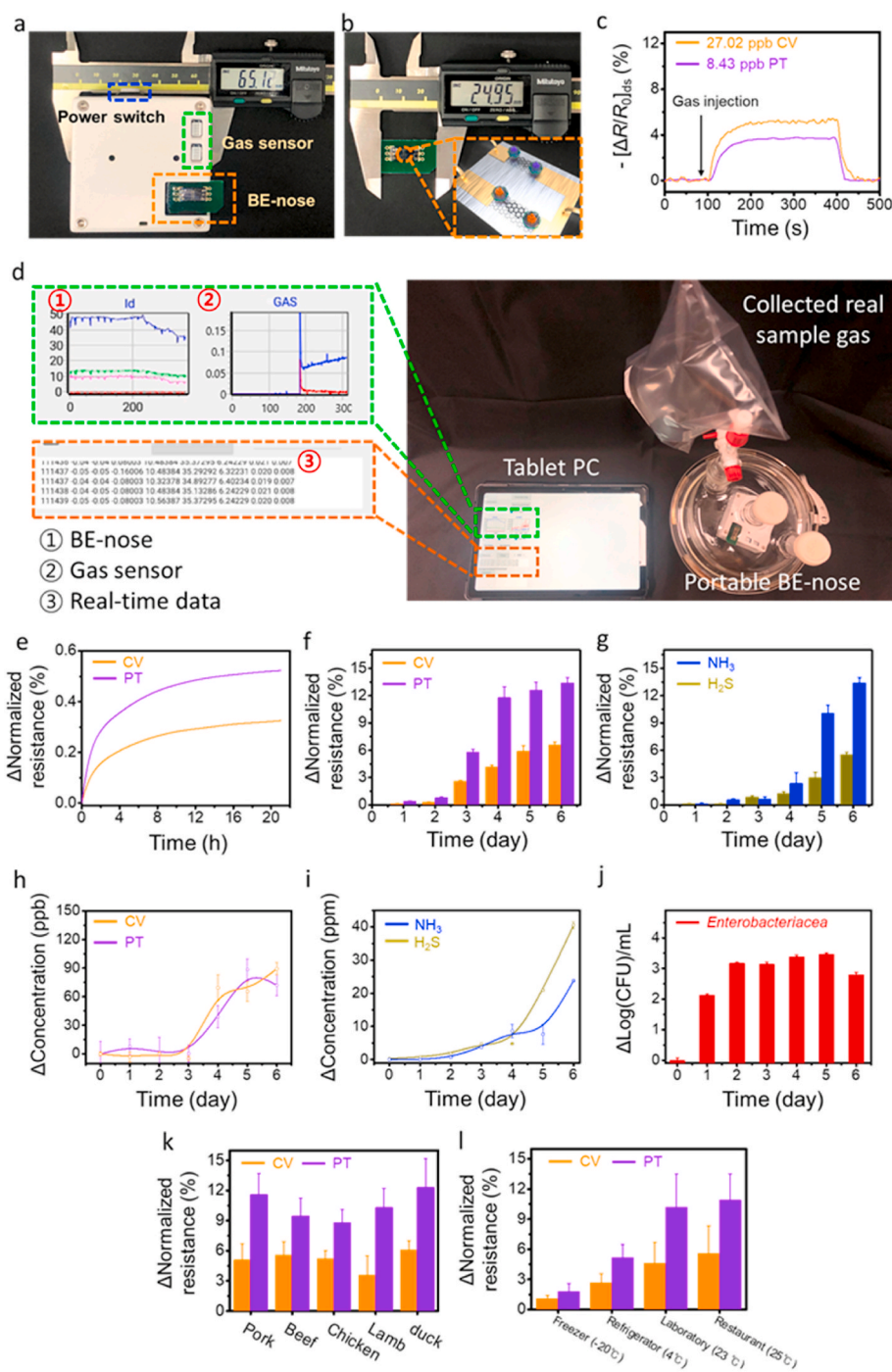


Fig. 6. Measurements of real samples using a portable BE-nose. **a, b** Photograph of the portable TAAR13 NDs BE-nose platform; BE-nose (orange dot box), commercial gas sensor (green dot box), and Bluetooth module (yellow dot box). **c** Real-time response of portable BE-nose toward CV and PT. **d** Photograph of real-time measurement system using portable BE-nose with real sample gases (CV, PT, NH₃, H₂S). **e** Real-time responses of CV and PT in the chamber with a real sample for 1 day. **f** The measured sensitivity of the portable BE-nose for the gas collected from a real sample for 6 days. **g** Real-time response toward NH₃ and H₂S using the commercial gas sensor in a real sample. **h** CV/PT GC-MS and **i** H₂S/NH₃ results in the real sample stored for 6 days. **j** The counted bacteria from the real sample for 6 days. The measured sensitivity of portable BE-nose depending on the diverse **k** real samples stored at room temperature and **l** in various environments for 5 days.

for 6 days after collecting the real gas sample from the chamber in a Tedlar bag (Fig. 6h). Due to extremely low sensitivity of GC-FID toward NH₃ and H₂S, NH₃ was analyzed by Fourier transform-infrared (FT-IR) spectroscopy gas analysis, and H₂S was analyzed by proton transfer reaction time of flight mass spectrometry (PTR-ToF-MS) by directly connecting the Tedlar bag to the inlet. The concentration changes for CV and PT were hardly observed, and the concentrations were 175 and 325 ppb, respectively, for two days. In addition, the changes of concentration gradually increased up to approximately 90 ppb, with the concentrations of CV and PT being raised to 260 and 400 ppb, respectively. The concentrations of CV and PT instantly increased after 4 days, whereas the portable TAAR13 NDs BE-nose could detect changes in CV and PT after 3 days (Fig. 6f, h and S11a). In addition, the initial concentrations

of NH₃ and H₂S were 5-10-fold higher than those of CV and PT and started to increase after 3 days (Fig. 6i and S11b). Although the concentrations of NH₃ and H₂S were 100-fold higher than those of CV and PT, the portable TAAR13 NDs BE-nose could sensitively detect spoilage indicators (CV and PT) earlier than NH₃ and H₂S sensor.

To investigate the microbial content in meat, we incubated 25 g beef for 6 days at room temperature and performed a colony formation assay using Petrifilm™ (3 M Science) (Fig. 6j and S12). The number of *Enterobacteriaceae* in meat is proportional to the degree of spoilage and the quantity of CV and PT (Bover-Cid et al., 2009; Mayr et al., 2003; Pircher et al., 2007). *Enterobacteriaceae* counts in beef increased until day 8, after which time, the microbial counts decreased during the spoilage period. Before incubating the beef under the experimental

conditions (day 0), the *Enterobacteriaceae* counts were 5.2 log (CFU)/mL, which is an acceptable level (Zhao et al., 2015). However, the counts exceeded the threshold levels of 7 log (CFU)/mL at day 1 and increased to 9 log (CFU)/mL at day 8 (Fig. S12). These counts result in discoloration, strong off-odors and slime production of spoiled meat (Reid et al., 2017). As the *Enterobacteriaceae* counts increased during the spoilage period, the quantities of CV and PT also showed an increasing trend and the portable TAAR13 NDs BE-nose showed a gradually increasing trend for resistance changes to CV and PT (Fig. 6f, h and 6j). The portable TAAR13 NDs BE-nose could be applied for monitoring food freshness and spoilage by detecting the indicators for real-time.

To investigate the concentration changes in the diverse samples, a portable TAAR13 NDs BE-nose was exposed to the collected gases from various real samples, such as pork, beef, chicken, sheep, and duck, in a chamber for 4 days at room temperature (Fig. 6k). We determined that the various real samples were in the spoilage stage by using the portable TAAR13 NDs BE-nose. These results indicate that the portable TAAR13 NDs BE-nose can be utilized to monitor meat freshness/spoilage via the detection of CV and PT. In addition, to investigate the dependence of the sensitivity toward of CV and PT on the environment, a real sample was stored for 5 days at various temperatures, namely, 20°C, 4°C, 23°C, and 25°C (Fig. 6l). We determined that the real sample stored in the freezer (−20°C) remained fresh but the real samples stored in the refrigerator (4°C), laboratory (23°C) and restaurant (25°C) were in the spoilage state. Interestingly, a decrease in resistance was observed with decreasing temperature due to deactivation of the decarboxylase activity of microorganisms (Bunčková et al., 2010).

4. Conclusion

In this study, a portable BE-nose demonstrated excellent sensitivity and selectivity toward various indicators and spoilage gases and was used to monitor the freshness and spoilage state over time. The TAAR13 family was used for the detection of CV and PT due to possible selective recognition and was fabricated in ND form to enhance its environmental stability. TAAR13 NDs SG-FETs showed excellent sensitivity, with LODs of 1 fM and 1 fM for CV and PT, respectively, and selectively responded to the various markers in the liquid state. The mechanisms and binding affinities were demonstrated by comparing the binding energies via biosimulations, and the binding of TAAR13d with PT showed higher affinity than that of TAAR13c with CV. The TAAR13 NDs BE-nose showed excellent LODs of 26.48 and 7.29 ppb for CV and PT, respectively, and displayed unprecedented detection ability for the spoilage indicators VOC (volatile organic compound) and VBN (volatile basic nitrogen). Based on these technologies, the TAAR13 NDs BE-nose was developed as a portable device, and was utilized for monitoring the freshness of various real samples in various environments. The responses toward the indicators in the real sample were also detected in the fresh stage prior to spoilage. Finally, the portable TAAR13 NDs BE-nose platform was performed towards diverse on-site and the various real samples and was used to monitor the time of freshness. This bio-electronic nose can potentially be utilized for the in situ and on-site monitoring of meat spoilage.

CRedit authorship contribution statement

Kyung Ho Kim: Methodology, Validation, Writing – original draft, Writing – review & editing, Data curation. **Dongseok Moon:** Methodology, Validation, Writing – original draft, Writing – review & editing, Data curation. **Jai Eun An:** Methodology, Writing – original draft. **Seon Joo Park:** Validation. **Sung Eun Seo:** Formal analysis. **Siyoung Ha:** Software. **Jinyeong Kim:** Resources, Formal analysis. **Kayoung Kim:** Methodology. **Sooyeol Phyoo:** Methodology. **Jiwon Lee:** Methodology. **Hye-Yeon Kim:** Resources. **Moonil Kim:** Resources. **Tai Hyun Park:** Writing – review & editing, Conceptualization, Supervision, Project administration, Funding acquisition. **Hyun Seok Song:** Writing – review

& editing, Conceptualization, Supervision, Project administration, Funding acquisition. **Oh Seok Kwon:** Writing – review & editing, Conceptualization, Supervision, Project administration, Funding acquisition.

Declaration of competing interest

The authors declare that they have no known competing financial interests or personal relationships that could have appeared to influence the work reported in this paper.

Acknowledgements

This research was supported by the Korea Basic Science Institute grant (C130000); the Korea Institute of Science and Technology (KIST) KIST institutional Program (2E31711); the National Research Foundation of Korea (NRF) funded by the Ministry of Science and ICT (MSIT) of Korea (2018R1A2B3004498); the European Research Council (ERC) under the European Union's Horizon 2020 research and innovation program (grant agreement no. 682286); Korea Institute of Planning and Evaluation for Technology in Food, Agriculture and Forestry(IPET) and Korea Smart Farm R&D Foundation(KosFarm) through Smart Farm Innovation Technology Development Program, funded by Ministry of Agriculture, Food and Rural Affairs(MAFRA) and Ministry of Science and ICT(MSIT), Rural Development Administration (RDA) (421020-03); the National Research Foundation of Korea (NRF) funded by the Ministry of Science and ICT (NRF-2020M3E9A1111636); the Bio & Medical Technology Development Program of the National Research Foundation (NRF) funded by the Ministry of Science & ICT (NRF-2021M3A9I5021439); the National R&D Program of National Research Foundation of Korea (NRF) funded by Ministry of Science and ICT (NRF-2021M3H4A4079381); the National Research Council of Science and Technology (NST) grant by the Korea Government (CRC22021-300); the Korea Research Institute of Bioscience and Biotechnology(KRIBB) Research Initiative Program (KGM2112234).

Appendix B. Supplementary data

Supplementary data to this article can be found online at <https://doi.org/10.1016/j.bios.2022.114551>.

References

- Biasini, M., Bienert, S., Waterhouse, A., Arnold, K., Studer, G., Schmidt, T., Kiefer, F., Cassarino, T.G., Bertoni, M., Bordoli, L., Schwede, T., 2014. SWISS-MODEL: modelling protein tertiary and quaternary structure using evolutionary information. *Nucleic Acids Res.* 42, W252–W258.
- Bover-Cid, S., Izquierdo-Pulido, M., Carmen Vidal-Carou, M., 2001. Changes in biogenic amine and polyamine contents in slightly fermented sausages manufactured with and without sugar. *Meat Sci.* 57, 215–221.
- Bover-Cid, S., Torriani, S., Gatto, V., Tofalo, R., Suzzi, G., Belletti, N., Gardini, F., 2009. Relationships between microbial population dynamics and putrescine and cadaverine accumulation during dry fermented sausage ripening. *J. Appl. Microbiol.* 106, 1397–1407.
- Bunčková, L., Buňka, F., Mantlová, G., Čablová, A., Sedláček, I., Švec, P., Pachlová, V., Kráčmar, S., 2010. The effect of ripening and storage conditions on the distribution of tyramine, putrescine and cadaverine in Edam-cheese. *Food Microbiol.* 27, 880–888.
- Castrica, M., Panseri, S., Siletti, E., Borghonovo, F., Chiesa, L., Balzaretto, C.M., 2019. Evaluation of smart portable device for food diagnostics: a preliminary study on Cape Hake fillets (*M. Capensis* and *M. Paradoxus*). *J. Chem.* 1–7.
- Dave, D., Ghaly, A.E., 2011. Meat spoilage mechanisms and preservation techniques: a critical review. *Am. J. Agric. Biol. Sci.* 6, 486–510.
- De Las Rivas, B., Marcobal, Á., Carrascosa, A.V., Muñoz, R., 2006. PCR detection of foodborne bacteria producing the biogenic amines histamine, tyramine, putrescine, and cadaverine. *J. Food Protect.* 69, 2509–2514.
- Denisov, I.G., Sliigar, S.G., 2017. Nanodiscs in membrane biochemistry and biophysics. *Chem. Rev.* 117, 4669–4713.
- Denisov, I.G., Sliigar, S.G., 2016. Nanodiscs for structural and functional studies of membrane proteins. *Nat. Struct. Mol. Biol.* 23, 481–486.
- Draisci, R., Volpe, G., Lucentini, L., Cecilia, A., Federico, R., Palleschi, G., 1998. Determination of biogenic amines with an electrochemical biosensor and its application to salted anchovies. *Food Chem.* 62, 225–232.

- Fujimoto, T., Awaga, K., 2013. Electric-double-layer field-effect transistors with ionic liquids. *Phys. Chem. Chem. Phys.* 15, 8983–9006.
- Gialama, D., Delivoria, D.C., Michou, M., Giannakopoulou, A., Skretas, G., 2017a. Functional requirements for DjlA- and RraA-mediated enhancement of recombinant membrane protein production in the engineered *Escherichia coli* strains SuptoxD and SuptoxR. *J. Mol. Biol.* 429, 1800–1816.
- Gialama, D., Kostelidou, K., Michou, M., Delivoria, D.C., Kolisis, F.N., Skretas, G., 2017b. Development of *Escherichia coli* strains that withstand membrane protein-induced toxicity and achieve high-level recombinant membrane protein production. *ACS Synth. Biol.* 6, 284–300.
- Goddard, A.D., Dijkman, P.M., Adamson, R.J., Dos Reis, R.I., Watts, A., 2015. Reconstitution of membrane proteins: a GPCR as an example. *Methods Enzymol.* 556, 405–424.
- Hagn, F., Nasr, M.L., Wagner, G., 2018. Assembly of phospholipid nanodiscs of controlled size for structural studies of membrane proteins by NMR. *Nat. Protoc.* 13, 79–98.
- Halász, A., Baráth, Á., Simon-Sarkadi, L., Holzapfel, W., 1994. Biogenic amines and their production by microorganisms in food. *Trends Food Sci. Technol.* 5, 42–49.
- Heim, B., Handrick, R., Hartmann, M.D., Kiefer, H., 2021. Refolding and characterization of two G protein-coupled receptors purified from *E. coli* inclusion bodies. *PLoS One* 16 e0247689–e0247689.
- Hussain, A., Saraiva, L.R., Ferrero, D.M., Ahuja, G., Krishna, V.S., Liberles, S.D., Korsching, S.I., 2013. High-affinity olfactory receptor for the death-associated odor cadaverine. *Proc. Natl. Acad. Sci. U. S. A* 110, 19579–19584.
- Jairath, G., Singh, P.K., Dabur, R.S., Rani, M., Chaudhari, M., 2015. Biogenic amines in meat and meat products and its public health significance: a review. *J. Food Sci. Technol.* 52, 6835–6846.
- Johansen, N.T., Tidemand, F.G., Nguyen, T.T.T.N., Rand, K.D., Pedersen, M.C., Arleth, L., 2019. Circularized and solubility-enhanced MSPs facilitate simple and high-yield production of stable nanodiscs for studies of membrane proteins in solution. *FEBS J.* 286, 1734–1751.
- Kaale, L.D., Eikevik, T.M., Rustad, T., Kolsaker, K., 2011. Superchilling of food: a review. *J. Food Eng.* 107, 141–146.
- Kiefer, H., Krieger, J., Olszewski, J.D., Von Heijne, G., Prestwich, G.D., Breer, H., 1996. Expression of an olfactory receptor in *Escherichia coli*: purification, reconstitution, and ligand binding. *Biochemistry* 35, 16077–16084.
- Kim, H., Trinh, B.T., Kim, K.H., Moon, J., Kang, H., Jo, K., Akter, R., Jeong, J., Lim, E.K., Jung, J., Choi, H.S., Park, H.G., Kwon, O.S., Yoon, I., Kang, T., 2021. Au@ZIF-8 SERS paper for food spoilage detection. *Biosens. Bioelectron.* 179, 113063.
- Kim, K.H., An, J.E., Kim, J.-S., Bae, J., Kwon, O.S., 2021. Graphene field-effect transistor based high-performance wireless portable device for H1N1 detection. *Appl. Sci. Converg. Technol.* 30, 111–114.
- Kim, K.H., Lee, S.H., Seo, S.E., Bae, J., Park, S.J., Kwon, O.S., 2020a. Ultrasensitive stress biomarker detection using polypyrrole nanotube coupled to a field-effect transistor. *Micromachines* 11, 439.
- Kim, K.H., Park, S.J., Park, C.S., Seo, S.E., Lee, J., Kim, J., Lee, Seung Hwan, Lee, S., Kim, J.-S., Ryu, C.-M., Yong, D., Yoon, H., Song, H.S., Lee, Sang Hun, Kwon, O.S., 2020b. High-performance portable graphene field-effect transistor device for detecting Gram-positive and -negative bacteria. *Biosens. Bioelectron.* 167, 112514.
- Kim, T., Moon, D., Park, J.H., Yang, H., Cho, S., Park, T.H., Ahn, D.J., 2019. Visual detection of odorant geraniol enabled by integration of a human olfactory receptor into polydiacetylene/lipid nano-assembly. *Nanoscale* 11, 7582–7587.
- Kwon, O.S., Lee, S.H., Park, S.J., An, J.H., Song, H.S., Kim, T., Oh, J.H., Bae, J., Yoon, H., Park, T.H., Jang, J., 2013. Large-scale graphene micropattern nano-biohybrids: high-performance transducers for FET-type flexible fluidic HIV immunoassays. *Adv. Mater.* 25, 4177–4185.
- Kwon, O.S., Song, H.S., Park, S.J., Lee, S.H., An, J.H., Park, J.W., Yang, H., Yoon, H., Bae, J., Park, T.H., Jang, J., 2015. An ultrasensitive, selective, multiplexed superbioelectronic nose that mimics the human sense of smell. *Nano Lett.* 15, 6559–6567.
- Lee, B.Y., Sung, M.G., Lee, J., Baik, K.Y., Kwon, Y.K., Lee, M.S., Hong, S., 2011. Universal parameters for carbon nanotube network-based sensors: can nanotube sensors be reproducible? *ACS Nano* 5, 4373–4379.
- Lee, S.H., Kim, K.H., Seo, S.E., Kim, M. il, Park, S.J., Kwon, O.S., 2020. Cytochrome C-decorated graphene field-effect transistor for highly sensitive hydrogen peroxide detection. *J. Ind. Eng. Chem.* 83, 29–34.
- Leopold, J., Abu-Hanna, A., Colombo, C., Sterk, P., Schultz, M., Bos, L., 2016. Factors influencing continuous breath signal in intubated and mechanically-ventilated intensive care unit patients measured by an electronic nose. *Sensors* 16, 1337.
- Li, H., Fang, J., Wei, X., Xu, D., Zhang, T., Xiang, Y., Chen, H.J., Liu, F., Xie, X., Wang, P., Hu, N., 2020. Specific recognition of ion channel blocker by high-content cardiomyocyte electromechanical integrated correlation. *Biosens. Bioelectron.* 162, 112273.
- Li, Q., Tachie-Baffour, Y., Liu, Z., Baldwin, M.W., Kruse, A.C., Liberles, S.D., 2015. Non-classical amine recognition evolved in a large clade of olfactory receptors. *Elife* 4.
- Li, Y.R., Matsunami, H., 2011. Activation state of the M3 muscarinic acetylcholine receptor modulates mammalian odorant receptor signaling. *Sci. Signal.* 4.
- Liberles, S.D., 2015. Trace amine-associated receptors: ligands, neural circuits, and behaviors. *Curr. Opin. Neurobiol.* 34, 1–7.
- Liberles, S.D., 2009. Trace amine-associated receptors are olfactory receptors in vertebrates. In: *Annals of the New York Academy of Sciences*, pp. 168–172.
- Ma, J., Lu, Y., Wu, D., Peng, Y., Loa-Kum-Cheung, W., Peng, C., Quinn, R.J., Shui, W., Liu, Z.J., 2017. Ligand identification of the adenosine A2A receptor in self-assembled nanodiscs by affinity mass spectrometry. *Anal. Methods* 9, 5851–5858.
- Ma, Z., Chen, P., Cheng, W., Yan, K., Pan, L., Shi, Y., Yu, G., 2018. Highly sensitive, printable nanostructured conductive polymer wireless sensor for food spoilage detection. *Nano Lett.* 18, 4570–4575.
- Mayr, D., Margesin, R., Klingsbichel, E., Hartungen, E., Jenewein, D., Schinner, F., Märk, T.D., 2003. Rapid detection of meat spoilage by measuring volatile organic compounds by using proton transfer reaction mass spectrometry. *Appl. Environ. Microbiol.* 69, 4697–4705.
- Michou, M., Kapsalis, C., Pliotas, C., Skretas, G., 2019. Optimization of recombinant membrane protein production in the engineered *Escherichia coli* strains SuptoxD and SuptoxR. *ACS Synth. Biol.* 8, 1631–1641.
- Morsy, M.K., Zór, K., Kostasheva, N., Alstrom, T.S., Heiskanen, A., El-Tanahi, H., Sharoba, A., Papkovsky, D., Larsen, J., Khalaf, H., Jakobsen, M.H., Emnéus, J., 2016. Development and validation of a colorimetric sensor array for fish spoilage monitoring. *Food Control* 60, 346–352.
- Nimsuk, N., 2019. Improvement of accuracy in beer classification using transient features for electronic nose technology. *J. Food Meas. Char.* 13, 656–662.
- Oh, J., Yang, H., Jeong, G.E., Moon, D., Kwon, O.S., Physo, S., Lee, J., Song, H.S., Park, T. H., Jang, J., 2019a. Ultrasensitive, selective, and highly stable bioelectronic nose that detects the liquid and gaseous cadaverine. *Anal. Chem.* 91, 12181–12190.
- Oh, J., Yang, H., Jeong, G.E., Moon, D., Kwon, O.S., Physo, S., Lee, J., Song, H.S., Park, T. H., Jang, J., 2019b. Ultrasensitive, selective, and highly stable bioelectronic nose that detects the liquid and gaseous cadaverine. *Anal. Chem.* 91, 12181–12190.
- Park, S.J., Lee, J., Seo, S.E., Kim, K.H., Park, C.S., Lee, S.H., Ban, H.S., Lee, B.D., Song, H. S., Kim, J., Lee, C.S., Bae, J., Kwon, O.S., 2020. High-performance conducting polymer nanotube-based liquid-ion gated field-effect transistor aptasensor for dopamine exocytosis. *Sci. Rep.* 10, 3772.
- Park, S.J., Seo, S.E., Kim, K.H., Lee, Sang Hun, Kim, J., Ha, S., Song, H.S., Lee, Seung Hwan, Kwon, O.S., 2021. Real-time monitoring of geosmin based on an aptamer-conjugated graphene field-effect transistor. *Biosens. Bioelectron.* 174, 112804.
- Pircher, A., Bauer, F., Paulsen, P., 2007. Formation of cadaverine, histamine, putrescine and tyramine by bacteria isolated from meat, fermented sausages and cheeses. *Eur. Food Res. Technol.* 226, 225–231.
- Reid, R., Fanning, S., Whyte, P., Kerry, J., Lindqvist, R., Yu, Z., Bolton, D., 2017. The microbiology of beef carcasses and primals during chilling and commercial storage. *Food Microbiol.* 61, 50–57.
- Rouck, J.E., Krapf, J.E., Roy, J., Huff, H.C., Das, A., 2017. Recent advances in nanodisc technology for membrane protein studies (2012–2017). *FEBS Lett.* 591, 2057–2088.
- Ruiz-Capillas, C., Herrero, A.M., 2019. Impact of biogenic amines on food quality and safety. *Foods* 8, 62.
- Rukchon, C., Nopwinyuwong, A., Trevanich, S., Jinkarn, T., Suppakul, P., 2014. Development of a food spoilage indicator for monitoring freshness of skinless chicken breast. *Talanta* 130, 547–554.
- Saito, H., Chi, Q., Zhuang, H., Matsunami, H., Mainland, J.D., 2009. Odor coding by a mammalian receptor repertoire. *Sci. Signal.* 2 ra9–ra9.
- Schaude, C., Meindl, C., Fröhlich, E., Attard, J., Mohr, G.J., 2017. Developing a sensor layer for the optical detection of amines during food spoilage. *Talanta* 170, 481–487.
- Semeano, A.T.S., Maffei, D.F., Palma, S., Li, R.W.C., Franco, B.D.G.M., Roque, A.C.A., Gruber, J., 2018. Tilapia fish microbial spoilage monitored by a single optical gas sensor. *Food Control* 89, 72–76.
- Serebryany, E., Zhu, G.A., Yan, E.C.Y., 2012. Artificial membrane-like environments for in vitro studies of purified G-protein coupled receptors. *Biochim. Biophys. Acta Biomembr.* 1818, 225–233.
- Shalaby, A.R., 1996. Significance of biogenic amines to food safety and human health. *Food Res. Int.* 29, 675–690.
- Shao, C., Zheng, H., Zhou, Z., Li, J., Lou, X., Hui, G., Zhao, Z., 2018. Ridgetail white prawn (*Exopalaemon carinicauda*) K value predicting method by using electronic nose combined with non-linear data analysis model. *Food Anal. Methods* 11, 3121–3129.
- Sharma, K., Ahuja, G., Hussain, A., Balfanz, S., Baumann, A., Korsching, S.I., 2016. Elimination of a ligand gating site generates a supersensitive olfactory receptor. *Sci. Rep.* 6.
- Sharma, K., Balfanz, S., Baumann, A., Korsching, S., 2018. Full rescue of an inactive olfactory receptor mutant by elimination of an allosteric ligand-gating site. *Sci. Rep.* 8, 1–11.
- Siripongpreta, T., Siralertmukul, K., Rodthongkum, N., 2020. Colorimetric sensor and LD1-MS detection of biogenic amines in food spoilage based on porous PLA and graphene oxide. *Food Chem.* 329, 127165.
- Son, M., Kim, D., Ko, H.J., Hong, S., Park, T.H., 2017. A portable and multiplexed bioelectronic sensor using human olfactory and taste receptors. *Biosens. Bioelectron.* 87, 901–907.
- Triki, M., Herrero, A.M., Jiménez-Colmenero, F., Ruiz-Capillas, C., 2018. Quality assessment of fresh meat from several species based on free amino acid and biogenic amine contents during chilled storage. *Foods* 7.
- Valdez, M., Gupta, S.K., Lozano, K., Mao, Y., 2019. ForceSpun polydiacetylene nanofibers as colorimetric sensor for food spoilage detection. *Sens. Actuators, B* 297, 126734.
- Wadsäter, M., Maric, S., Simonsen, J.B., Mortensen, K., Cardenas, M., 2013. The effect of using binary mixtures of zwitterionic and charged lipids on nanodisc formation and stability. *Soft Matter* 9, 2329–2337.
- Wang, H., Li, H., Wei, X., Zhang, T., Xiang, Y., Fang, J., Wu, P., Xie, X., Wang, P., Hu, N., 2021. Recognition of high-specificity hERG K⁺ channel inhibitor-induced arrhythmia in cardiomyocytes by automated template matching. *Microsyst. Nanoeng.* 7, 24.
- Wang, L.G., Tonggu, L.G., 2015. Membrane protein reconstitution for functional and structural studies. *Sci. China Life Sci.*

- Xu, D., Fang, J., Zhang, M., Xia, Q., Li, H., Hu, N., 2022. Porous polyethylene terephthalate nanotemplate electrodes for sensitive intracellular recording of action potentials. *Nano Lett.* 22, 2479–2489.
- Xu, X.Y., Lian, X., Hao, J.N., Zhang, C., Yan, B., 2017. A double-stimuli-responsive fluorescent center for monitoring of food spoilage based on dye covalently modified EuMOFs: from sensory hydrogels to logic devices. *Adv. Mater.* 29, 1702298.
- Xu, Z., Li, Q., 2020. TAAR agonists. *Cell. Mol. Neurobiol.* 40, 257–272.
- Yang, H., Kim, D., Kim, J., Moon, D., Song, H.S., Lee, M., Hong, S., Park, T.H., 2017. Nanodisc-based bioelectronic nose using olfactory receptor produced in *Escherichia coli* for the assessment of the death-associated odor cadaverine. *ACS Nano* 11, 11847–11855.
- Yang, H., Song, H.S., Ahn, S.R., Park, T.H., 2015. Purification and functional reconstitution of human olfactory receptor expressed in *Escherichia coli*. *Biotechnol. Bioeng.* 20, 423–430.
- Ying, X., Zinnai, A., Venturi, F., Sanmartin, C., Deng, S., 2017. Freshness evaluation of grass carp (*Ctenopharyngodon idellus*) by electronic nose. *J. Food Meas. Char.* 11, 1026–1034.
- Zhao, F., Zhou, G., Ye, K., Wang, S., Xu, X., Li, C., 2015. Microbial changes in vacuum-packed chilled pork during storage. *Meat Sci.* 100, 145–149.
- Zheng, L., Zhang, J., Yu, Y., Zhao, G., Hui, G., 2016. Spinyhead croaker (*Collichthys lucidus*) quality determination using multi-walled carbon nanotubes gas-ionization sensor array. *J. Food Meas. Char.* 10, 247–252.
- Zhuang, H., Matsunami, H., 2008. Evaluating cell-surface expression and measuring activation of mammalian odorant receptors in heterologous cells. *Nat. Protoc.* 3, 1402–1413.
- Zhuang, H., Matsunami, H., 2007. Synergism of accessory factors in functional expression of mammalian odorant receptors. *J. Biol. Chem.* 282, 15284–15293.